

Article

PtPd Hybrid Composite Catalysts as Cathodes for Proton Exchange Membrane Fuel Cells

Yazmín Yorely Rivera-Lugo ¹, Kevin Isaac Pérez-Muñoz ¹, Balter Trujillo-Navarrete ¹, Carolina Silva-Carrillo ¹, Edgar Alonso Reynoso-Soto ¹, Julio Cesar Calva Yañez ², Shui Wai Lin ¹, José Roberto Flores-Hernández ³ and Rosa María Félix-Navarro ^{1,*}

¹ Tecnológico Nacional de Mexico, Instituto Tecnológico de Tijuana, Centro de Graduados e Investigación en Química, Blvd. Alberto Limón Padilla, s/n, Otay Tecnológico, Tijuana 22510 B.C., Mexico; yazrl@hotmail.com (Y.Y.R.-L.); kevinperez5@gmail.com (K.I.P.-M.); balter.trujillo@tectijuana.edu.mx (B.T.-N.); caro.silva.carrillo@gmail.com (C.S.-C.); edgar.alonso@tectijuana.mx (E.A.R.-S.); sl388@aol.com (S.W.L.)

² CONACYT-Tecnológico Nacional de Mexico, I.T. Tijuana, Centro de Graduados e Investigación en Química, Blvd. Alberto Limón Padilla, s/n, Otay Tecnológico, Tijuana 22510 B.C., Mexico; jcalva@conacyt.mx

³ Instituto Nacional de Electricidad y Energías Limpias, Ave. Reforma 113 Col. Palmira, Cuernavaca 62490, Morelos, Mexico; jrflores@ineel.mx

* Correspondence: rmfelix@tectijuana.mx; Tel.: +52-664-623-4043

Received: 28 November 2019; Accepted: 5 January 2020; Published: 9 January 2020



Abstract: In this work, PtPd hybrid cathodic catalysts were prepared for a proton exchange membrane fuel cell (PEMFC) application by two different strategies. The first strategy was the physical mixing of bimetallic PtPd onto partially reduced graphene oxide (PtPd/rGO) and PtPd onto multi-walled carbon nanotubes (PtPd/MWCNT); (PtPd/rGO) + (PtPd/MWCNT). The second strategy was physical mixing of both carbonaceous supports before the PtPd deposition to form PtPd/(rGO:MWCNT). Our experimental results revealed that the PtPd nanomaterial prepared over a mixture of both carbonaceous supports had better oxygen reduction reaction (ORR) and PEMFC performances than the individually prepared catalysts. The insertion of MWCNT between rGO sheets prevented their stacking. This promoted the diffusion of oxygen molecules through the interlayer spacing, enhancing the ORR's electrocatalytic activity. The durability test demonstrated that the hybrid supporting material dramatically improved the catalyst's stability even after 3000 reaction cycles. This highlighted an increase greater than 100% for hybrid nanocomposites in their electrocatalytic activity as compared with the PtPd/rGO nanocomposite.

Keywords: PtPd; supported electrocatalyst; MWCNT; graphene; ORR; PEMFC

1. Introduction

Energy demand is a global concern. As the world's population grows, energy production also increases [1]. Nowadays, energy is mainly derived from fossil fuels. Fossil fuel combustion is the primary source of greenhouse gases, which modifies the Earth's climate, the atmosphere, and the ocean. A key aspect of the solution is renewable energy production free of anthropogenic CO₂ [2–6].

Recently, researchers have shown an increased interest in the development of fuel cells as an option for green power generation [7]. One of them is the proton exchange membrane fuel cell (PEMFC), where a hydrogen oxidation reaction (HOR, Equation (1)) takes place at the anode and an oxygen reduction reaction (ORR, Equation (2)) occurs at the cathode.





The main disadvantage of PEMFCs is given by the ORR, which is the limiting reaction [8]. One solution is the use of metallic catalysts that allow for improving the ORR's efficiency. Among these, Pt has better catalytic performance because it has a suitable oxygen binding energy [9]. Recent studies suggest that bimetallic catalysts, such as PtAu [10], PtIr [11], PtRu [12], and PtPd [13,14], can further improve the oxygen binding energy as compared to single-Pt catalysts. In those cases, the selection of the carbonaceous support is crucial for a metallic catalyst. The support must be chemically stable in order to prevent corrosion, as well as be an excellent electrical conductor, e.g., multi-walled carbon nanotubes (MWCNT) [15,16] and graphene [17,18]. Calderón et al. reported the synthesis of a PtPd/carbon black catalyst, and they found that the addition of Pd modifies the interatomic distance of PtPt; this effect promotes H₂O formation instead of H₂O₂ [19], which is a desirable feature for PEMFC applications. A recent work by Fu et al. reported a PtPd nanorods electrocatalyst for the ORR, employing a mixture of partially reduced graphene oxide (rGO) and MWCNTs as a support, and they determined that the synergistic effect of both carbon nanomaterials notably improves the stability of the PtPd alloy electrocatalyst [20]. The use of carbonaceous materials as spacers in graphene layers is a strategy that has been used in order to increase the ORR's activity [21–23]; however, there has been no systematic investigation on the effect of the physical mixing of hybrid electrocatalysts.

In this work, we prepared two different PtPd systems. The first one was prepared by physical mixing of individual catalysts, PtPd/rGO and PtPd/MWCNT (50:50 wt.%), to obtain the hybrid electrocatalyst (PtPd/rGO) + (PtPd/MWCNT). The second system was created by mixing the carbonaceous supports (50:50 wt.% of rGO:MWCNT) physically before the PtPd deposition to obtain the electrocatalyst PtPd/(rGO:MWCNT). Then, the catalytic activity of both systems was compared for the ORR in the half-cell test and PEMFC applications. It is suggested that the strategy of mixing the supports before PtPd deposition is the best choice for synthesizing carbon nanostructured hybrids of PtPd with better catalytic activity.

2. Materials and Methods

The MWCNTs were prepared by the spray pyrolysis method according to the procedure reported by Reyes-Cruzaley et al. [24]. Graphene oxide was prepared by the modified Hummers method proposed by Tour et al. [25], with minor modifications. In summary, 3 mg of graphite was placed in H₂SO₄ (conc.) and oxidized with NaNO₃ and KMnO₄, then H₂O and H₂O₂ were added to the reaction mixture. For purification, the product was washed with HCl (5 vol%) and water until the pH was 7. The final product was collected and dried in a stove at 60 °C for 12 h. All aqueous solutions were prepared with Milli-Q[®] water (18 MΩ).

2.1. Synthesis of PtPd Nanoparticles (NPs) Supported on Carbonaceous Nanomaterials

A two-step reaction was carried out. The first step consisted of the deposition of metallic Pd nanoparticles on the carbon supports by the microemulsion method, which contained 0.098 M of CTAB dissolved in a mixture of isopropanol:water (14:1 vol. ratio). After the carbon support (rGO, MWCNT, or rGO:MWCNT) was dispersed into the solution, the obtained dispersion was heated at 60 °C under constant stirring. Then, a microemulsion solution was added into the support dispersion, containing 81.4 mmol of NaBH₄ and 69.2 mmol of sodium citrate. Next, an aqueous solution of 0.129 mmol Na₂PdCl₄ was prepared and added to the resulting solution to be incorporated into the reaction flask; the reaction mixture was left to react for 3 h. The final product was filtered and washed with isopropanol, water, and acetone, and dried at 60 °C overnight. The second step comprised the incorporation of Pt metal, using the same methodology as the first step, changing only the concentration of Pt metallic precursor, which was 0.052 mmol of K₂PtCl₆; the new support was a Pd/carbonaceous support. Finally, PtPd/MWCNTs support was subject to a heat treatment at 300 °C in an argon atmosphere for 30 min.

2.2. Physical Mixing of Carbonaceous Supports for the Synthesis of PtPd/(rGO:MWCNT) Electrocatalysts

The rGO and MWCNT supports were mixed in a 50:50 weight ratio, as reported in the literature [26,27]. After that, the procedure above, mentioned in Section 2.1, was followed to obtain the PtPd/(rGO:MWCNT) electrocatalysts.

2.3. Physical Mixing of Electrocatalysts to Obtain (PtPd/rGO) + (PtPd/MWCNT)

For the comparison of electrocatalysts prepared on different carbonaceous supports, the electrocatalysts PtPd/rGO and PtPd/MWCNT were prepared and physically mixed with a 50:50 weight ratio to obtain the analogous (PtPd/rGO) + (PtPd/MWCNT) electrocatalyst. The procedure was to mix the individual electrocatalysts (PtPd/rGO and PtPd/MWCNT), and disperse them in 5 mL of methanol for 2.5 min under sonication, followed by filtration and drying in an oven at 60 °C overnight.

2.4. Physicochemical and Electrochemical Characterization

Several techniques were used in the characterization of the carbonaceous support powders. The thermal behavior and metallic content were investigated by thermogravimetric analysis (TGA) using a TA Instruments Q500. The thermograms were obtained at a heat rate of 20 °C·min⁻¹ up to 900 °C with an air flow of 40 mL·min⁻¹. The metallic composition was determined by inductively coupled plasma optical emission spectroscopy (ICP-OES) by a Perkin-Elmer Optima 8300, where 5 mg of solid samples were calcinated and dissolved in aqua regia. The morphology of NPs was studied by transmission electron microscopy (TEM) using a JEOL JEM-2200FS microscope with a spherical aberration corrector in the probe mode, working at 200 kV. The structural composition of the membrane electrode assemblies (MEAs) was evaluated by scanning electron microscopy (SEM). The micrographs were acquired with a TESCAN model VEGA3 scanning electron microscope, operated at 20 kV. A potentiostat/galvanostat Bio-Logic instruments model VMP-300 was used for all of the electrochemical tests, and as electrolyte, an aqueous solution 0.5 M H₂SO₄. The electrochemical experiments were performed in a three-electrode cell arrangement (25 ± 1 °C): (1) the reference electrode was Ag/AgCl/NaCl_(sat); (2) a Pt wire was used as a counter electrode; and (3) a glassy carbon rotating disk electrode with an area of 0.2 cm² was used as a working electrode (WE). This area was modified using catalytic inks that were prepared with 2 mg of the synthesized catalysts, dispersed in 550 µL of ethanol, and 150 µL of Nafion[®], where the WE was modified using 0.114 mg of the electrocatalyst. Cyclic voltammograms were obtained in a potential range from -225 to 1240 mV versus Ag/AgCl/NaCl_(sat) with a scan rate of 100 mV·s⁻¹. The catalytic activity evaluation in the ORR was performed by linear sweep voltammetry at 5 mV·s⁻¹, and at different rotation speeds of 0, 100, 250, 500, 750, 1000, and 1600 rpm, controlled by a Pine Instruments part number AFMSRCE rotator, where the electrolyte was O₂-saturated. Accelerated durability tests (ADT) were carried out by continuous cyclic voltammograms and ORR measurements at 0 and 3000 cycles, under the same conditions as previously described. All potentials were reported versus the standard hydrogen electrode (SHE).

2.5. PEMFC Performance Test

MEAs were prepared following the methodology proposed in a previous report [10]. Bimetallic catalysts and hybrid nanocomposites (PtPd/rGO, PtPd/MWCNT, (PtPd/rGO) + (PtPd/MWCNT), and PtPd/(rGO:MWCNT)), were used to modify the cathode gas diffusion layer (GDL). For comparison, a catalyst loading of 30 mg was kept in all MEAs. The preparation of MEA consisted of spraying the catalytic ink solution onto the GDL (surface area: 9 cm²) and a commercial Nafion[®] NRE-212 membrane was used as a separator for the cathode and anode diffusers. The MEA was pressed at 0.4 ton·cm² at 120 °C for 2 min. The protocol for the fuel cell tests was similar to that previously reported [8,28]. PEMFC performance tests were performed in custom-made single fuel cell hardware. A potentiostat/galvanostat Solartron, model 1287, with a 20 A booster, was employed to obtain the polarization curves at an operation temperature of 60 °C. The electrical resistance of the assemblies

was measured by electrochemical impedance spectroscopy (EIS) using a Solartron potentiostat model 1290 and an impedance/gain-phase analyzer. In all tests, O₂ was employed and commercial (20%) Pt/C was used as a catalyst in the anode gas diffuser, which was obtained from the Fuel Cell Store.

3. Results and Discussion

3.1. Physicochemical Characterization

Figure 1 shows the thermal behavior of the carbonaceous supports and electrocatalysts for the study of their weight loss curves (wt.%). In the case of the rGO support, it showed three decomposition stages. The first stage represents 5%, which is observed in the range from 40 to 100 °C, and is related to the desorption of moisture [29]. The second stage has the highest weight loss (82%) at 205 °C and corresponds to the decomposition of oxygenated groups [30]. The final stage corresponds to 10% at 550 °C, and is associated with the decomposition of the carbon network [31]. The final residue of 3% was attributed to potassium salts. In the case of the MWCNT support, two stages are observed. The first one (1%) at 200 °C is due to the decomposition of oxygenated groups [32], while the second one (93%) between 550 and 650 °C is related to the decomposition of the carbon skeleton [31]. The metallic residue was 5%, corresponding to the Fe₂O₃ that was used as a growth seed in the synthesis of MWCNTs.

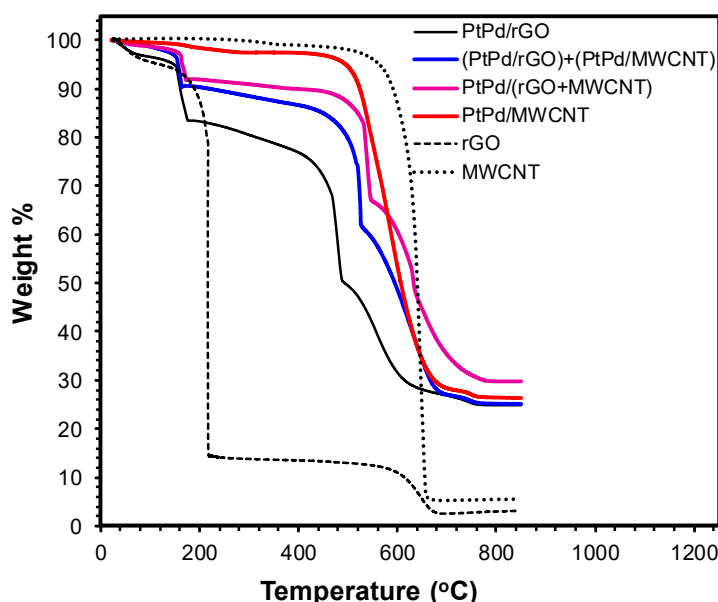


Figure 1. Thermal behavior of carbonaceous supports (partially reduced graphene oxide (rGO) and multi-walled carbon nanotubes (MWCNTs)), bimetallic nanomaterials (PtPd/rGO and PtPd/MWCNT), and hybrid nanomaterials: ((PtPd/rGO) + (PtPd/MWCNT) and PtPd/(rGO:MWCNT)).

The electrocatalysts showed the weight loss associated with the linked support and, in the case of PtPd/MWCNT, the thermogram showed, additionally, a step between 160 and 250 °C, which is related to the residual surfactant molecules, while the metal residue was 26.33%. Since TGA does not differentiate between metals, it was necessary to perform an ICP analysis, showing 7.39% for Pt and 10.62% for Pd. In the case of PtPd/rGO, the metal residue was 24.84%, being 8.74% of Pt and 12.60% of Pd. For (PtPd/rGO) + (PtPd/MWCNT), the metal residue obtained was 25.12%, with the following composition: 7.45% of Pt and 11.81% of Pd. Finally, PtPd(rGO:MWCNT) presented a metallic residue of 29.76%, and the composition was 7.18% of Pt and 16.20% of Pd.

Figure 2a shows the micrographs of PtPd/rGO and Figure 2b shows the micrograph of PtPd/MWCNT. PtPd NPs are well-dispersed on both surfaces, showing a small number of agglomerates. Also, the average NP diameter was calculated using image analysis; the size distribution values of the PtPd/rGO and PtPd/MWCNT electrocatalysts were 16 ± 4 nm and 12 ± 5 nm, respectively.

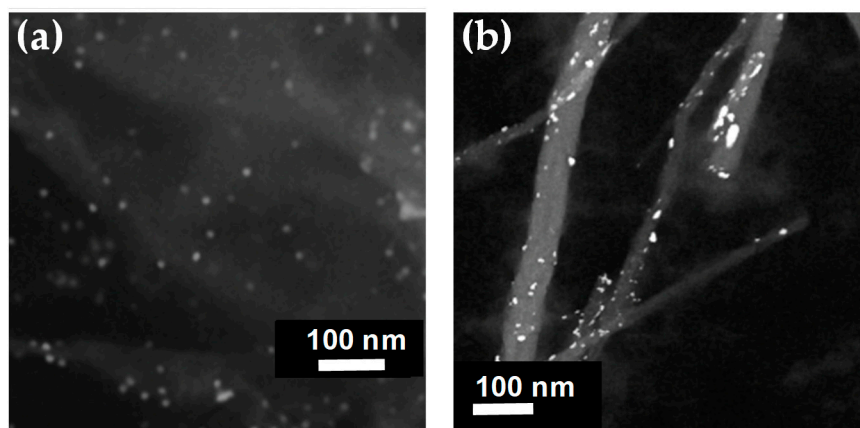


Figure 2. Transmission electron microscopy (TEM) micrographs of: (a) PtPd/rGO; and (b) PtPd/MWCNT.

3.2. Electrochemical Characterization

The ORR's activity was analyzed for PtPd electrocatalysts as a part of the electrochemical performance evaluation, employing linear sweep voltammetry (LSV) and a rotating disk electrode (RDE). Figure 3 shows the results of this study. The ORR mechanism involves different pathways in acidic media [33]; one of them is the generation of H_2O_2 by two transferred electrons, or H_2O by four transferred electrons. In order to clarify the electrons involved in the reaction, the Koutecký–Levich equation (Equation (3)) was used.

$$\frac{1}{j_L} = \frac{1}{nFC_0k} + \frac{1}{0.62nFC_0D^{2/3}v^{-1/6}\omega^{1/2}} \quad (3)$$

where n is the number of transferred electrons, F is the Faraday constant, C_0 is the saturated oxygen concentration, D is the diffusion coefficient of oxygen, ν is the kinematic viscosity of the electrolyte, ω is the rotation speed (radians per second), and k is the electron-transfer rate constant. The slope of the graphic represents n .

In the inset of Figure 3d, it can be seen that all of the nanomaterials prepared in this work followed a four-electron pathway, generating water, making them ideal candidates to be tested as cathodic catalysts in a PEMFC.

Figure 4 shows the comparison of the electroactivity of catalysts for the ORR at 1600 rpm, where it is noticeable that PtPd/rGO had the lowest limiting current density at 1600 rpm and 0.2 V versus SHE ($-1.88 \text{ mA}\cdot\text{cm}^{-2}$). PtPd/MWCNT presented a value of $-6.73 \text{ mA}\cdot\text{cm}^{-2}$, while (PtPd/rGO) + (PtPd/MWCNT) and PtPd(rGO:MWCNT) had very similar values of -7.06 and $-7.18 \text{ mA}\cdot\text{cm}^{-2}$, respectively. As for the onset potential, the electrocatalyst based on mixing of supports had a more positive value than electrocatalysts supported on rGO or MWCNT, with values of 0.75 V for PtPd/rGO, 0.78 V for PtPd/MWCNT, 0.80 V for (PtPd/rGO) + (PtPd/MWCNT), and 0.86 V for PtPd(rGO:MWCNT). From Figure 4, it is established that both hybrid nanocomposites had a better ORR performance than the bimetallic catalysts.

The low ORR activity for PtPd/rGO can be explained on the basis that partially reduced graphene, prepared by chemical reduction of graphene oxide, is known to have lower electron conductivity (around 100–200 S/m) than MWCNT (10,000 S/m) [34]. Also, graphene tends to restack due to its strong Van der Waals interactions [35], avoiding appropriate oxygen transportation to active sites [36]. The improvement in catalytic activity for the physical mixing of the catalysts may be the reason that the addition of PtPd/MWCNT to PtPd/rGO causes an increase in the accessibility of PtPd on MWCNT, resulting in a better catalytic response of the NPs in the mixture, increasing the available triple-phase boundaries (gas–electrolyte–catalyst). Additionally, MWCNTs prevent the rGO from restacking, promoting the PtPd supported on rGO to be involved in the electrochemical reactions on electrodes because of the triple-phase boundaries [37,38]. In addition, when electrocatalysts supported

in the mixture of rGO:MWCNT were tested, they showed better electroactivity. This might be due to the fact that MWCNTs can form conductive paths between graphene layers [39,40], and at the same time graphene fills voids among MWCNTs, providing a lower junction resistance between rGO and MWCNTs [41], increasing the conductivity of the supported composite [35,42]. Furthermore, MWCNTs prevent graphene from restacking [43,44], facilitating O₂ transport and mass transfer.

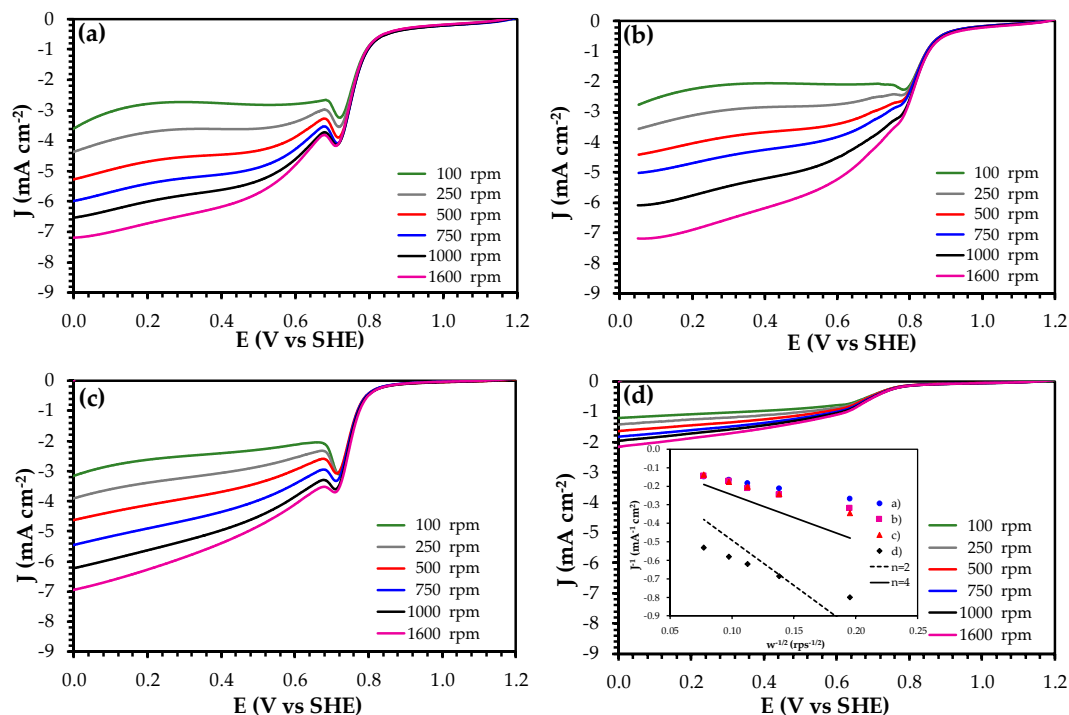


Figure 3. Linear voltammograms of (a) (PtPd/rGO) + (PtPd/MWCNT), (b) PtPd/(rGO:MWCNT), (c) PtPd/MWCNT, and (d) PtPd/rGO (inset: comparison of Koutecky–Levich plots at 0.2 V versus a standard hydrogen electrode (SHE) for all electrocatalysts) recorded in O₂-saturated H₂SO₄ (0.5 M) at 5 mV·s⁻¹ and different rotation rates.

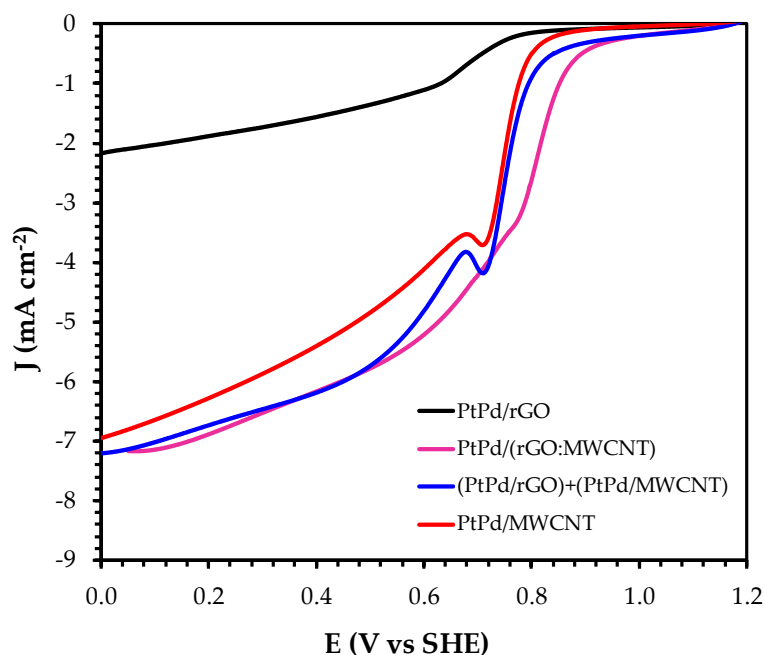


Figure 4. Comparison at 1600 rpm of linear voltammograms in O₂-saturated H₂SO₄ (0.5 M) at 5 mV·s⁻¹ for PtPd/rGO, PtPd/MWCNT, (PtPd/rGO) + (PtPd/MWCNT), and PtPd/(rGO:MWCNT).

3.3. PEMFC Test

The PtPd-supported electrocatalysts were used to modify the cathodic gas diffuser in order to be tested in a hydrogen fuel cell. The polarization and power density curves are shown in Figure 5. It can be seen that PtPd/rGO had a low catalytic activity with a current density of 99 mA·cm⁻² at 0.6 V ($P_{max} = 90 \text{ mW}\cdot\text{cm}^{-2}$). In contrast, the other bimetallic catalyst, PtPd/MWCNT, showed a current density of 319 mA·cm⁻² at 0.6 V ($P_{max} = 280 \text{ mW}\cdot\text{cm}^{-2}$). As expected from the ORR experiments, PtPd electrocatalysts supported in the mixture of rGO:MWCNT showed a better current density, with experimental data of 337 mA·cm⁻² at 0.6 V ($P_{max} = 306 \text{ mW}\cdot\text{cm}^{-2}$) for (PtPd/rGO) + (PtPd/MWCNT) and 351 mA·cm⁻² at 0.6 V ($P_{max} = 337 \text{ mW}\cdot\text{cm}^{-2}$) for PtPd(rGO:MWCNT). This agreed with the results in the half-cell, where the PtPd electrocatalyst with the physical mixing of carbonaceous supports had a better catalytic response towards the ORR. In Table 1, we compare different PtPd materials as cathodes in a PEMFC. We can see that our catalyst showed a better response than most of them, even without optimizing the ionomer content in the catalytic layer, which is a determining factor in the catalytic response of the fuel cell, because of the interaction between the ionomer and the nanoparticles [45,46].

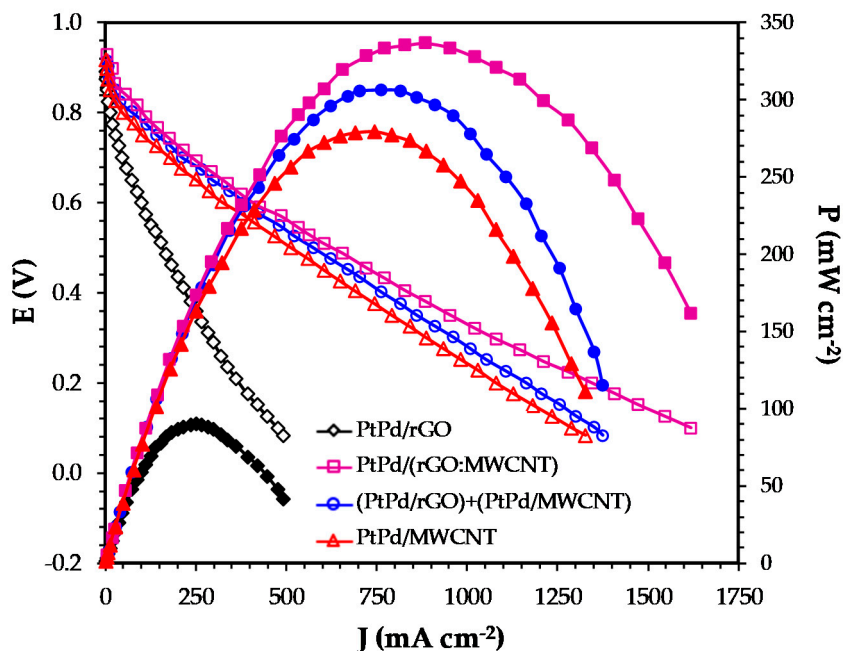


Figure 5. Polarization and power density curves of PtPd/rGO, PtPd/MWCNT, PtPd/(rGO:MWCNT), and (PtPd/rGO) + (PtPd/MWCNT).

Table 1. Comparison of Proton Exchange Membrane Fuel Cell (PEMFC) performance of different PtPd materials as cathodes.

Reference	Current Density at 0.6 V (mA/cm ²)	Material	Metal Loading (wt.%)	% Pt	% Pd	Pt Loading in MEA (mg/cm ²)	Operating Temperature (°C)
This work	351	PtPd/(rGO:MWCNT)	23.38	7.18	16.2	0.5	60
[47]	236	PtPd/C	31.47	15.92	15.55	0.1	170
[48]	265	PtPd/HCMS	20	15	5	0.4	70
[49]	424.4	PtPd/C	23.8	3.02	20.78	0.3	65
[50]	150	PtPd/C	60	3	57	0.2	70

SEM micrographs of the cathode gas diffuser modified with PtPd electrocatalysts in MEA are shown in Figure 6. The MEA of PtPd/rGO showed a small catalytic layer with a thickness of 2 μm, which explains the low ORR activity in the hydrogen fuel cell: due to the compact layer, there is no suitable gas transport to the catalytic sites. In the case of PtPd/MWCNT-MEA, this presented a catalytic layer with a thickness of 19 μm; however, the layer was uneven. The cathode of (PtPd/rGO) + (PtPd/MWCNT) also had an irregular layer, but it had a thickness of 21 μm. Finally, PtPd(rGO:MWCNT)-MEA showed

a uniform catalyst layer of 14 μm . Due to the acceptable catalyst layer thickness, and the large contact area between the gases and the PtPd NPs of the last three materials, these were expected to have a good gas transport, i.e., a good catalytic activity in the PEMFC, which they had [8].

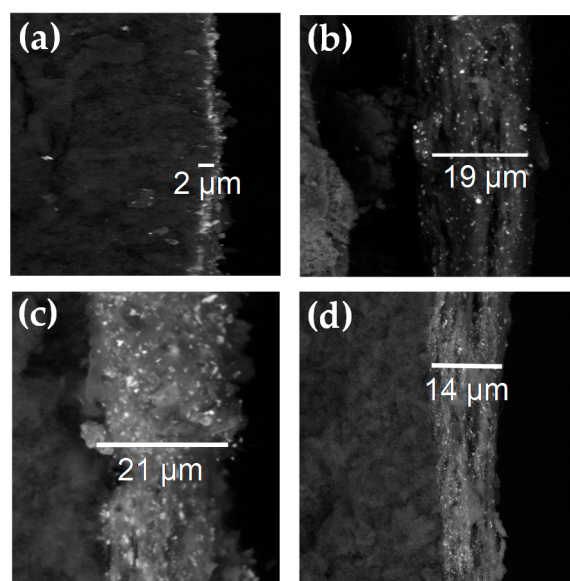


Figure 6. Scanning electron microscopy (SEM) micrographs of the membrane electrode assemblies (MEAs) catalytic layer of: (a) PtPd/rGO; (b) PtPd/MWCNT; (c) (PtPd/rGO) + (PtPd/MWCNT); and (d) PtPd(rGO:MWCNT).

3.4. Accelerated Durability Tests (ADT)

Excellent stability is a desirable feature for application in a PEMFC, so we carried out accelerated durability tests (ADT). The results are shown in Figure 7. These tests consisted of the application of 3000 cyclic voltammograms to report the specific activity of catalysts at 0.5 V versus SHE. PtPd/rGO had poor stability at the end of the test, maintaining 37% of its initial activity towards the ORR. It has been reported that the loss of catalytic activity could be due to several factors, such as Pt dissolution, Pt mobility (leading to particle growth), and support corrosion [51]. Anson et al. established that a decrease in the thickness of the catalytic layer results in a decrease in the limiting current [52], which makes us assume that our catalyst is dissolving into the electrolyte. Likewise, PtPd supported in the mixture of rGO:MWCNT improved the stability of PtPd/rGO, keeping 95% for (PtPd/rGO) + (PtPd/MWCNT), and 96% for PtPd(rGO:MWCNT). Among all catalysts, PtPd/MWCNT showed the best retention of activity at 3000 cycles, decreasing only 1% of the initial specific activity. It can be noticed that the catalyst supported on rGO had the worst stability, while the catalyst deposited on MWCNTs had the best, and the hybrids presented intermediate stabilities. This leads us to think that rGO is suffering from corrosion, which blocks oxygen diffusion into catalytic sites [53]. When MWCNTs are in the hybrid catalysts, they provide an improvement in stability, reducing corrosion and stacking of the rGO, and generating a better mass transfer [20,53].

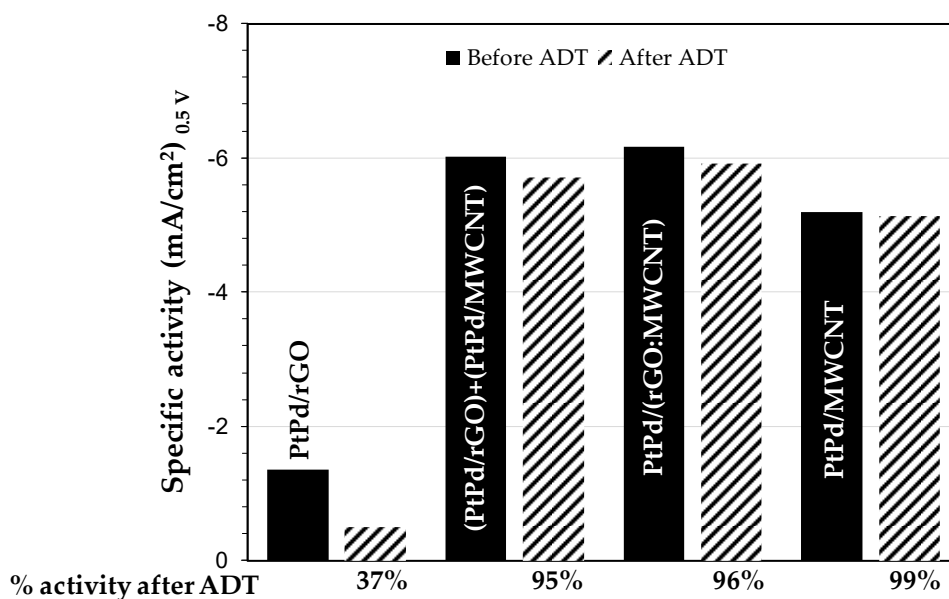


Figure 7. Stability results of bimetallic catalysts and hybrid nanocomposites.

4. Conclusions

In summary, we synthesized PtPd hybrid catalysts by two different routes: by the physical mixing of individual catalysts ((PtPd/rGO) + (PtPd/MWCNT)), and by mixing of carbonaceous supports before the metallic deposition (PtPd/(rGO:MWCNT)). Both strategies improved more than 3 times the catalytic activity of PtPd/rGO and exceeded the PtPd/MWCNT performance in the PEMFC; however, the second approach, PtPd/(rGO:MWCNT), showed better performance. The insertion of MWCNTs between rGO sheets prevented them from restacking, promoted diffusion of oxygen molecules through the rGO sheets, and enhanced the ORR electrocatalytic activity in the PEMFC.

Author Contributions: Y.Y.R.-L. and K.I.P.-M. are Ph.D. and Master's students, respectively, who developed much of the experimental methodology. Y.Y.R.-L. prepared the original draft. B.T.-N. performed the characterization of the membrane electrode assemblies by scanning electron microscopy. C.S.-C. and E.A.R.-S. applied the methodology for catalyst synthesis. J.C.C.Y. made some electrochemical characterizations. S.W.L. wrote, reviewed, and edited the manuscript. J.R.F.-H. performed the studies in the PEMFC. R.M.F.-N. worked on the visualization, supervision, and administration of the project, funding acquisition, and wrote the manuscript. All authors have read and agreed to the published version of the manuscript.

Funding: This research was funded by CONACYT from Mexico (National Council for Science and Technology), grant number: CB-2014-240498, and TecNM (National Technology of Mexico), grant number 6306.19-P.

Acknowledgments: The authors wish to thank the Advanced Materials Research Center (CIMAV), and Potosino Institute of Scientific and Technological Research (IPICYT), for providing the facility for the TEM analysis.

Conflicts of Interest: The authors declare no conflicts of interest.

References

- Zach, F.; Kretschmer, F.; Stoeglehner, G. Integrating energy demand and local renewable energy sources in smart urban development zones: New options for climate-friendly resilient urban planning. *Energies* **2019**, *12*, 3672. [CrossRef]
- Armeanu, D.Ş.; Gherghina, Ş.C.; Pasmangiu, G. Exploring the causal nexus between energy consumption environmental pollution and economic growth: Empirical evidence from central and eastern Europe. *Energies* **2019**, *12*, 3704. [CrossRef]
- Chub, A.; Vinnikov, D.; Stepenko, S.; Liivik, E.; Blaabjerg, F. Photovoltaic energy yield improvement in two-stage solar microinverters. *Energies* **2019**, *12*, 3774. [CrossRef]

4. Jiménez-Buendía, F.; Villena-Ruiz, R.; Honrubia-Escribano, A.; Molina-García, Á.; Gómez-Lázaro, E. Submission of a WECC DFIG wind turbine model to Spanish operation procedure 12.3. *Energies* **2019**, *12*, 3749. [[CrossRef](#)]
5. Jidin, R.; Othman, A.B. A computed river flow-based turbine controller on a programmable logic controller for run-off river hydroelectric systems. *Energies* **2017**, *10*, 1717. [[CrossRef](#)]
6. Cadelano, G.; Cicolin, F.; Emmi, G.; Mezzasalma, G.; Poletto, D.; Galgaro, A.; Bernardi, A. Improving the energy efficiency, limiting costs and reducing CO₂ Emissions of a museum using geothermal energy and energy management policies. *Energies* **2019**, *12*, 3192. [[CrossRef](#)]
7. Yahhoub, M.; Jamalabadi, A.; Ghasemi, M.; Alamian, R.; Afshari, E.; Wongwises, S.; Rashidi, M.M.; Shadloo, M.S. A 3D simulation of single-channel high-temperature polymer exchange membrane fuel cell performances. *Appl. Sci.* **2019**, *9*, 3633. [[CrossRef](#)]
8. Rivera-Lugo, Y.Y.; Salazar-Gastélum, M.I.; López-Rosas, D.M.; Reynoso-Soto, E.A.; Pérez-Sicairos, S.; Velraj, S.; Flores-Hernández, J.R. Effect of template, reaction time and platinum concentration in the synthesis of PtCu/CNT catalyst for PEMFC applications. *Energy* **2018**, *148*, 561–570. [[CrossRef](#)]
9. Norskov, J.K.; Rossmeisl, J.; Logadottir, A.; Lindqvist, L. Origin of the overpotential for oxygen reduction at a fuel-cell cathode. *J. Phys. Chem. B* **2004**, *108*, 17886–17892. [[CrossRef](#)]
10. Beltrán-Gastélum, M.; Salazar-Gastélum, M.I.; Flores-Hernández, J.R.; Botte, G.G.; Pérez-Sicairos, S.; Romero-Castañón, T.; Reynoso-Soto, E.A.; Félix-Navarro, R.M. Pt-Au nanoparticles on graphene for oxygen reduction reaction: Stability and performance on proton exchange membrane fuel cell. *Energy* **2019**, *181*, 1225–1234. [[CrossRef](#)]
11. Todoroki, N.; Watanabe, H.; Kondo, T.; Kaneko, S.; Wadayama, T. Highly enhanced oxygen reduction reaction activity and electrochemical stability of Pt/Ir(111) bimetallic surfaces. *Electrochim. Acta* **2016**, *222*, 1616–1621. [[CrossRef](#)]
12. Jackson, A.; Strickler, A.; Higgins, D.; Jaramillo, T.F. Engineering Ru@Pt core-shell catalysts for enhanced electrochemical oxygen reduction mass activity and stability. *Nanomaterials* **2018**, *8*, 38. [[CrossRef](#)]
13. Tang, Y.; Chen, T.; Guo, W. Surfactant-free synthesis of reduced graphene oxide supported well-defined polyhedral Pd-Pt nanocrystals for oxygen reduction reaction. *Catalysts* **2019**, *9*, 756. [[CrossRef](#)]
14. Cai, Z.-X.; Liu, C.-C.; Wu, G.-H.; Chen, X.-M.; Chen, X. Green synthesis of Pt-on-Pd bimetallic nanodendrites on graphene via in situ reduction, and their enhanced electrocatalytic activity for methanol oxidation. *Electrochim. Acta* **2014**, *127*, 377–383. [[CrossRef](#)]
15. Mirzaei, F.; Parnian, M.J.; Rowshanzamir, S. Durability investigation and performance study of hydrothermal synthesized platinum-multi walled carbon nanotube nanocomposite catalyst for proton exchange membrane fuel cell. *Energy* **2017**, *138*, 696–705. [[CrossRef](#)]
16. Matsuda, N.; Nakashima, T.; Kato, T.; Shiroishi, H. Synthesis of multiwall carbon nanotube-supported platinum catalysts by solution plasma processing for oxygen reduction in polymer electrolyte fuel cells. *Electrochim. Acta* **2014**, *146*, 73–78. [[CrossRef](#)]
17. Fortunato, G.; de Lima, F.; Maia, G. Oxygen-reduction reaction strongly electrocatalyzed by Pt electrodeposited onto graphene or graphene nanoribbons. *J. Power Sources* **2016**, *302*, 247–258. [[CrossRef](#)]
18. Pothaya, S.; Regalbuto, J.R.; Monnier, J.R.; Punyawudho, K. Preparation of Pt/graphene catalysts for polymer electrolyte membran fuel cells by strong electrostatic adsorption technique. *Int. J. Hydrog. Energy* **2019**, *44*, 26361–26372. [[CrossRef](#)]
19. Calderón, J.C.; Ndzuzo, L.; Bladergroen, B.J.; Pasupathi, S. Catalytic activity of carbon supported-Pt-Pd nanoparticles toward the oxygen reduction reaction. *Mater. Today Proc.* **2018**, *5*, 10551–10560. [[CrossRef](#)]
20. Fu, K.; Wang, Y.; Mao, L.; Yang, X.; Jin, J.; Yang, S.; Li, G. Facile morphology controllable synthesis of PtPd nanorods on graphene-multiwalled carbon nanotube hybrid support as efficient electrocatalysts for oxygen reduction reaction. *Mater. Res. Bull.* **2018**, *108*, 187–194. [[CrossRef](#)]
21. Yang, H.N.; Lee, D.C.; Park, K.W.; Kim, W.J. Platinum-boron doped graphene intercalated by carbon black for cathode catalyst in proton exchange membrane fuel cell. *Energy* **2015**, *89*, 500–510. [[CrossRef](#)]
22. Sanli, L.I.; Yazar, B.; Bayram, V.; Gürsel, S.A. Electrospayed catalyst layers based on Graphene-carbon black hybrids for the next-generation fuel cell electrodes. *J. Mater. Sci.* **2017**, *52*, 2091–2102. [[CrossRef](#)]
23. Yang, H.N.; Ko, Y.D.; Kim, W.J. 3-D structured Pt/rGO-polyethyleneimine-functionalized MWCNT for proton exchange membrane fuel cell. *Int. J. Hydrog. Energy* **2018**, *43*, 4439–4447. [[CrossRef](#)]

24. Reyes-Cruzaley, A.P.; Félix-Navarro, R.M.; Trujillo-Navarrete, B.; Silva-Carrillo, C.; Zapata-Fernández, J.R.; Romo-Herrera, J.M.; Contreras, O.E.; Reynoso-Soto, E.A. Synthesis of novel Pd NP-PTH-CNTs hybrid materials as catalyst for H₂O₂ generation. *Electrochim. Acta* **2019**, *296*, 575–581. [[CrossRef](#)]
25. Marcano, D.C.; Kosynkin, D.V.; Berlin, J.M.; Sinitskii, A.; Sun, Z.; Slesarev, A.; Alemany, L.B.; Lu, W.; Tour, J.M. Improved synthesis of graphene oxide. *ACS Nano* **2010**, *4*, 4806–4814. [[CrossRef](#)]
26. Ratso, S.; Kruusenberg, I.; Joost, U.; Saar, R.; Tammeveski, K. Enhanced oxygen reduction reaction activity of nitrogen-doped graphene/multi-walled carbon nanotube catalysts in alkaline media. *Int. J. Hydrog. Energy* **2016**, *41*, 22510–22519. [[CrossRef](#)]
27. Zhang, J.; Song, X.; Li, P.; Wu, Z.; Wu, Y.; Wang, S.; Liu, X. Sulfur, nitrogen co-doped nanocomposite of graphene and carbon nanotube as an efficient bifunctional electrocatalyst for oxygen reduction and evolution reactions. *J. Taiwan Inst. Chem. Eng.* **2018**, *93*, 336–341. [[CrossRef](#)]
28. Beltrán-Gastélum, M.; Salazar-Gastélum, M.I.; Félix-Navarro, R.M.; Pérez-Sicairos, S.; Reynoso-Soto, E.A.; Lin, S.W.; Flores-Hernández, J.R.; Romero-Castañón, T.; Albarrán-Sánchez, I.L.; Paraguay-Delgado, F. Evaluation of PtAu/MWCNT (multiwalled carbon nanotubes) electrocatalyst performance as cathode of a proton exchange membrane fuel cell. *Energy* **2016**, *109*, 446–455. [[CrossRef](#)]
29. Jeong, H.K.; Lee, Y.P.; Lahaye, R.J.W.E.; Park, M.H.; An, K.H.; Kim, I.J.; Yang, C.W.; Park, C.Y.; Ruoff, R.S.; Lee, Y.H. Evidence of nearly flat layers and AB stacking order of graphite oxides. *J. Am. Chem. Soc.* **2008**, *130*, 1362–1366. [[CrossRef](#)]
30. Jeong, H.-K.; Lee, Y.P.; Jin, M.H.; Kim, E.S.; Bae, J.J.; Lee, Y.H. Thermal stability of graphite oxide. *Chem. Phys. Lett.* **2009**, *470*, 255–258. [[CrossRef](#)]
31. Andersen, S.M.; Borghei, M.; Lund, P.; Elina, Y.-R.; Pasanen, A.; Kauppinen, E.; Ruiz, V.; Kauranen, P.; Skou, E.M. Durability of carbon nanofiber (CNF) & carbon nanotube (CNT) as catalyst support for Proton Exchange Membrane Fuel Cells. *Solid State Ion.* **2013**, *231*, 94–101. [[CrossRef](#)]
32. Wepasnick, K.A.; Smith, B.A.; Schrote, K.E.; Wilson, H.K.; Diegelmann, S.R.; Fairbrother, D.H. Surface and structural characterization of multi-walled carbon nanotubes following different oxidative treatments. *Carbon* **2011**, *49*, 24–36. [[CrossRef](#)]
33. Katsounaros, I.; Schneider, W.B.; Meier, J.C.; Benedikt, U.; Biedermann, P.U.; Auer, A.A.; Mayrhofer, K.J.J. Hydrog. peroxide electrochemistry on platinum: Towards understanding the oxygen reduction reaction mechanism. *Phys. Chem. Chem. Phys.* **2012**, *14*, 7384–7391. [[CrossRef](#)] [[PubMed](#)]
34. Cheng, Q.; Tang, J.; Ma, J.; Zhang, H.; Shinya, N.; Qin, L.-C. Graphene and carbon nanotube composite electrodes for supercapacitors with ultra-high energy density. *Phys. Chem. Chem. Phys.* **2011**, *13*, 17615–17624. [[CrossRef](#)]
35. Yan, J.; Wei, T.; Shao, B.; Ma, F.; Fan, Z.; Zhang, M.; Zheng, C.; Shang, Y.; Qian, W.; Wei, F. Electrochemical properties of graphene nanosheet /carbon black composites as electrodes for supercapacitors. *Carbon* **2010**, *48*, 1731–1737. [[CrossRef](#)]
36. Hyuck, C.; Wook, M.; Chang, H.; Hoon, J.; Ihl, S. Applied catalysis B : Environmental nitrogen-doped graphene/carbon nanotube self-assembly for efficient oxygen reduction reaction in acid media. *Appl. Catal. B Environ.* **2014**, *144*, 760–766. [[CrossRef](#)]
37. Shaijumon, M.M.; Ramaprabhu, S. Platinum/multiwalled carbon nanotubes-platinum/carbon composites as electrocatalysts for oxygen reduction reaction in proton exchange membrane fuel cell. *Appl. Phys. Lett.* **2006**, *88*, 253105. [[CrossRef](#)]
38. Matsumoto, T.; Komatsu, T.; Arai, K.; Yamazaki, T.; Kijima, M.; Shimizu, H.; Takasawa, Y.; Nakamura, J. Reduction of Pt usage in fuel cell electrocatalysts with carbon nanotube electrodes. *Chem. Commun.* **2004**, 840–841. [[CrossRef](#)]
39. Li, C.; Li, Z.; Zhu, H.; Wang, K.; Wei, J.; Li, X.; Su, P.; Zhang, H.; Wu, D. Graphene Nano-“patches” on a carbon nanotube network for highly transparent/conductive thin film applications. *J. Phys. Chem. C* **2010**, *114*, 14008–14012. [[CrossRef](#)]
40. Tung, V.C.; Chen, L.-M.; Allen, M.J.; Wassei, J.; Nelson, K.; Kaner, R.B.; Yang, Y. Low-temperature solution processing of graphene-carbon nanotube hybrid materials for high-performance transparent conductors. *Nano Lett.* **2009**, *9*, 1945–1955. [[CrossRef](#)]
41. King, P.J.; Khan, U.; Lotya, M.; De, S.; Coleman, J.N. Improvement of transparent conducting nanotube films by addition of small quantities of graphene. *ACS Nano* **2010**, *4*, 4238–4246. [[CrossRef](#)] [[PubMed](#)]

42. Shim, W.; Kwon, Y.; Jeon, S.-Y.; Yu, W.-R. Optimally conductive networks in randomly dispersed CNT: Graphene hybrids. *Sci. Rep.* **2015**, *5*, 16568–16578. [[CrossRef](#)] [[PubMed](#)]
43. Imran, J.R.; Arockiados, T.; Rajalakshmi, N.; Ramaprabhu, S. Nanostructured Pt disperse don graphene-multiwalled carbon nanotube hybrid nanomaterials as electrocatalyst for PEMFC. *J. Electrochem. Soc.* **2010**, *157*, B874–B879. [[CrossRef](#)]
44. Du, H.Y.; Wang, C.H.; Hsu, H.C.; Chang, S.T.; Huang, H.C.; Chen, L.C.; Chen, K.H. Graphene nanosheet-CNT hybrid nanostructure electrode for a proton exchange membrane fuel cell. *Int. J. Hydrog. Energy* **2012**, *37*, 18989–18995. [[CrossRef](#)]
45. Xing, W.; Yin, G.; Zhang, J. *Rotating Electrode Methods and Oxygen Reduction Electrocatalyst*; Elsevier: Amsterdam, The Netherlands, 2014; Chapter 3; p. 109.
46. Abedini, A.; Dabir, B.; Kalnasi, M. Experimental verification for simulation study of Pt/CNT nanostructured cathode catalyst layer for PEM fuel cells. *Int. J. Hydrog. Energy* **2012**, *37*, 8439–8450. [[CrossRef](#)]
47. Yusof, M.S.M.; Jalil, A.A.; Ahmad, A.; Triwahyono, S.; Othman, M.H.D.; Abdullah, T.A.T.; Firmansyah, M.L.; Setiabudi, H.D.; Johari, A.; Nabgan, W. Effect of Pt-Pd/C coupled catalyst loading and polybenzimidazole ionomer binder on oxygen reduction reaction in high temperature PEMFC. *Int. J. Hydrog. Energy* **2019**, *44*, 20760–20769. [[CrossRef](#)]
48. Ficicilar, B.; Bayrakceken, A.; Eroglu, I. Effect of Pd loading in Pd-Pt bimetallic catalysts doped into hollow core mesoporous shell carbon on performance of proton exchange membrane fuel cells. *J. Power Sources* **2009**, *193*, 17–23. [[CrossRef](#)]
49. Jung, D.H.; Bae, S.J.; Kim, S.J.; Nahm, K.S.; Kim, P. Effect of the Pt precursor on the morphology and catalytic performance of Pt-impregnated on Pd/C for the oxygen reduction reaction in polymer electrolyte fuel cells. *Int. J. Hydrog. Energy* **2011**, *36*, 9115–9122. [[CrossRef](#)]
50. Cho, Y.-H.; Choi, B.; Cho, Y.-H.; Park, H.-S.; Sung, Y.-E. Pd-based PdPt(19:1)/C electrocatalyst as an electrode in PEM fuel cell. *Electrochem. Commun.* **2007**, *9*, 378–381. [[CrossRef](#)]
51. Hussain, S.; Erikson, H.; Kongi, N.; Tarre, A.; Ritslaid, P.; Rahn, M.; Matisen, L.; Merisalu, M.; Sammelselg, V.; Tammeveski, K. Pt nanoparticles sputter-deposited on TiO₂/MWCNT composites prepared by atomic layer deposition: Improved electrocatalytic activity towards the oxygen reduction reaction and durability in acid media. *Int. J. Hydrog. Energy* **2018**, *43*, 4967–4977. [[CrossRef](#)]
52. Steiger, B.; Anson, F.C. Examination of Cobalt “picket fence” porphyrin and its complex with 1-methylimidazole as catalysts for the electroreduction of dioxygen. *Inorg. Chem.* **2000**, *39*, 4579–4585. [[CrossRef](#)]
53. Lu, Y.; Jiang, Y.; Chen, W. PtPd porous nanorods with enhanced electrocatalytic activity and durability for oxygen reduction reaction. *Nano Energy* **2013**, *2*, 836–844. [[CrossRef](#)]

